

Chondrules as fallout from vaporizing impacts in the solar nebula

Nick Choksi¹^{*}, Eugene Chiang^{1,2}, Harold C. Connolly Jr.³, Zack Gainsforth⁴, Andrew J. Westphal⁴

¹*Astronomy Department, Theoretical Astrophysics Center, and Center for Integrative Planetary Science, University of California, Berkeley, CA*

²*Department of Earth and Planetary Science, University of California, Berkeley, CA*

³*Department of Geology, School of Earth and Environment, Rowan University, Glassboro, NJ*

⁴*Space Sciences Laboratory, University of California, Berkeley, CA*

Released 1 October 2020

ABSTRACT

We consider how chondrules, once-molten mm-sized spheres filling the oldest meteorites, may have formed as the thermally processed fallout from planetesimal collisions in the primordial solar nebula. We focus on the cloud of hot and dense silicate vapor released from a collision, and its expansion into cold and rarefied nebular hydrogen. Collisional particle debris, including chondrule precursors, are entrained by the cloud and melted by it, via gas conduction and radiation emitted by dust grains that condense out of the cloud. Conduction and radiation lock vapor, dust, and proto-chondrules to a common temperature, which falls as the cloud expands. Latent heat released by condensation slows cooling at first, but eventually radiative losses hasten it so that all remaining vapor condenses, leaving behind a pressure-less cavity which nebular gas backfills. Particles that are not too large are swept back in; of these, those that are not too small can sediment at drag-limited terminal velocities onto the planetesimal remains before solar tides tear them away. Particles that re-agglomerate with their parent thus have a specific size range: ~ 1 mm in the asteroid belt, and ~ 10 μm in the proto-Kuiper belt, for nebular densities comparable to the minimum-mass solar nebula. Thermal histories of chondrules in asteroids, and chondrule-like particles in the short-period comet 81P/Wild-2, are reproduced for colliding planetesimals of order 100 km in radius, matching the dominant sizes of Solar System minor bodies. If asteroids were born big and nebular gas densities decayed monotonically, then our model predicts older chondrules have larger maximum sizes and cooled more slowly. Problems, including the efficiency of chondrule production and the origin of CAIs, are discussed.

Key words: meteorites, meteors, meteoroids; minor planets, asteroids: general; Kuiper belt: general; protoplanetary discs; planets and satellites: formation

1 INTRODUCTION

Underneath the fusion crusts of the most primitive stony meteorites lies a profusion of millimeter-sized igneous spheres. These chondrules, which can fill $\gtrsim 50\%$ of meteorite volumes, are among the oldest creations of the Solar System, with lead isotopic ages of 4.562–4.567 billion years, and near-solar compositions in refractory elements. Chondrule petrology indicates they were heated to melting temperatures for a period of a few minutes, and that they cooled

over hours to days. Their roundness indicates that proto-chondrules were heated while suspended in space, so that surface tension pulled their shapes into spheres. For reviews, see Connolly Jr. & Jones (2016) and Russell et al. (2018).

From the petrologic data we can infer some rough orders of magnitude characterizing the chondrule formation environment. The fact that chondrules were partially molten implies an ambient temperature $T \sim 2000$ K. A single chondrule radiating into vacuum at this temperature would cool off unacceptably fast, within seconds; therefore chondrules must have been immersed in, and kept warm by, a gas of high heat capacity, or a radiation bath maintained by an optically thick medium, or both. The former possibility is fur-

* E-mail: nchoksi@berkeley.edu

ther supported by the retention of volatile elements, principally sodium, within chondrules, requiring ambient Na partial pressures of order $\sim 10^{-3}$ bars while $T \sim 2000$ K (Alexander et al. 2008; Fedkin & Grossman 2013). Gas at 2000 K has a sound speed ranging from $c_s \sim 0.7$ to 3 km/s, depending on whether it is composed predominantly of hydrogen or metals. A characteristic length scale for the formation environment is given by the sound speed multiplied by the cooling time, $R \sim 4 \times 10^4 \text{ km} (c_s/\text{km s}^{-1})(t_{\text{cool}}/10 \text{ hr})$.

These scales, which describe a formation setting that was hot, pressurized, and compact, do not recall those of the solar nebula (a.k.a. the protoplanetary disc), which for the most part was cold ($\lesssim 300$ K), rarefied ($\lesssim 10^{-4}$ bar in hydrogen, and orders of magnitude less in other elements), and extensive (with disc scale heights $\gtrsim 10^7$ km; e.g. Williams & Cieza 2011; Armitage 2011). This mismatch argues against purely nebular processes for creating chondrules. Furthermore, the hydrogen-rich composition of the nebula does not provide the high oxygen fugacities (oxygen partial pressures) required to form the iron-rich silicates present in chondrules (e.g. Ebel & Grossman 2000; Grossman et al. 2008).

The comparatively small, fast, and energetic scales inferred from chondrule petrology may instead be compatible with collisions between planetesimals. Impacts at relative velocities $u_{\text{rel}} \sim \mathcal{O}(1 \text{ km/s})$ (for reference, orbital velocities are ~ 20 km/s around the Sun in the main asteroid belt at 3 au) heat rock to a temperature of $T \sim \mu m_p u_{\text{rel}}^2/k \sim \mathcal{O}(10^3 \text{ K})$, where $\mu \sim 30$ is the mean molecular weight of silicate gas, m_p is the proton mass, and k is Boltzmann’s constant. The durations of heating and cooling should scale with the sizes of the colliding planetesimals. For example, if the colliding bodies are $R_{\text{pl}} \sim \mathcal{O}(100 \text{ km})$ in size, we might expect the initial fireball to last the “smash-through” time of $R_{\text{pl}}/u_{\text{rel}} \sim \mathcal{O}(10^2 \text{ s})$, consistent with a minutes-long heating event. The collisional destruction of the bodies may release an expanding cloud of debris and vapor, the thermodynamics of which could conceivably reproduce chondrule cooling rates. Fleshing out this possibility with a quantitative model is a goal of this paper.

Support for a collisional origin for chondrules has been building, although the evidence is still circumstantial and/or model-dependent, and questions remain. Krot et al. (2005) found that CB chondrules crystallized 4–5 Myr after the formation of the oldest objects in the Solar System (calcium-aluminium-rich inclusions in CV chondrites) and argued that by this time, the solar nebula may have largely dissipated, ruling out a purely nebular origin. They pointed to the metal nodules (a.k.a. blebs) in CB chondrites, and the non-porphyritic textures of CB chondrules, as signatures of melt production and vapor condensation from a hypervelocity impact (one fast enough to shock compress solids and produce melt and vapor). Villeneuve et al. (2015) argued similarly, that numerous experimental constraints on chondrule formation, from cooling profiles, oxygen fugacities, and relict grains are best explained by interaction of solids with impact-generated vapor after planetesimal collisions.

Asphaug et al. (2011) pioneered numerical simulations of chondrule formation in planetesimal collisions, suggesting that chondrules may have formed as liquid droplets sprayed out in low velocity collisions between planetesimals with largely molten interiors. Sanders & Scott (2012) further advocated for this scenario, arguing that it can resolve many of the petrological difficulties which attend non-collisional

formation models. Johnson et al. (2015) showed that the colliding bodies need not (and should not) be molten: melt is created and jetted out of the impact site when solids collide at high enough speeds, $u_{\text{rel}} \gtrsim 2.5$ km/s. Droplet sizes were estimated to be on the order of 1–10 mm for impactor diameters of 100–1000 km (see also Johnson & Melosh 2014). For these same parameters, chondrule cooling rates of 100–3000 K/hr, compatible with empirical constraints, were inferred from radiative transfer modeling of the optically thick jet.

In the impact simulations of Johnson et al. (2015) and Wakita et al. (2017), only a small fraction of the initially solid colliding mass, on the order of a percent, is jetted out as melt. Whether this efficiency of melt production is adequate to re-process enough of the main asteroid belt into the chondrites sampled on Earth is unclear (for a quick and optimistic calculation, see the penultimate paragraph on page 340 of Johnson et al. 2015). The issue is tied to how the droplets re-agglomerate onto larger bodies, and how the asteroid belt as a whole evolves. One school of thought posits that the chondrules sprayed into space by one body are later re-accreted onto other bodies by their gravity abetted by nebular gas drag, a process called pebble accretion (Johansen et al. 2015; Hasegawa et al. 2016). Pebble accretion is lossy, however, with the overwhelming majority of solids drifting radially past potential accretors in the primordial nebula (Ormel 2017; Lin et al. 2018). The high volume-filling fraction of chondrules in chondritic meteorites (see table 1 of Weisberg et al. 2006) is a stringent test of any theory, and pebble accretion does not appear to explain why meteorite parent bodies would accrete predominantly chondrules and not other objects that may behave dynamically similarly in the nebula but possess fundamentally different petrologies. The latter include unmelted collisional fragments and solids that avoided collisional processing altogether.

Here we further explore a collisional genesis for chondrules. New developments in modeling shocked forsterite and silica demonstrate that vapor can be produced in abundance through hypervelocity impacts between planetesimals which are, at least in their outer layers, initially solid (Carter & Stewart 2020; Davies et al. 2020). Stewart et al. (2019b) suggested that the resulting hot silicate vapor cloud (also called a vapor plume) may be conducive to chondrule formation. We investigate this possibility by studying the dynamic and thermodynamic evolution of the cloud, including its interaction with the hydrogen of the solar nebula. By contrast to Johnson et al. (2015) and related studies, we do not rely on melt created by decompression heating at the impact site to form chondrules. Indeed, we do not model the impact dynamics at all. Instead we begin our analysis post-impact, assuming that a cloud of hot vapor has been released from the collision, and that this vapor contains debris, possibly initially solid. We study the subsequent evolution of this debris, in particular how it can be heated, and melted, by ambient vapor and radiation. Our goal is to determine the initial cloud conditions required to transform collisional debris into chondrules. Our hope is that the cloud properties we infer can later be mapped to the kinds of collisions—the target and impactor masses, and the impact velocities—that make chondrules.

As part of our study, we quantitatively sketch how the solid/liquid debris, swept outward at first by the expanding vapor cloud, may eventually gravitate back toward the col-

tionally disrupted planetesimal remains. Here there is the possibility that the aerodynamics of fallback permit only certain size particles to re-agglomerate, potentially explaining why chondrules have a narrow size distribution (for measurements, see, e.g. Friedrich et al. 2015), and why asteroid surface layers may be littered with chondrules (Weiss & Elkins-Tanton 2013).

Our treatment of the vapor cloud and of the solids embedded within it is zero-dimensional: we do not spatially resolve the cloud, but restrict our attention to its mean properties, e.g. density and temperature, and their evolution with time. Our model is similar in spirit to that of Dullemond et al. (2014, 2016), who considered the evolution of a cloud containing essentially only molten chondrules, and no vapor except what outgasses from the melt. We study the complementary problem of a pure vapor cloud in which solid/liquid particles are sparsely embedded, and extend the analysis to consider the possible late-time fallback of material (which would obviate pebble accretion).

The order-of-magnitude style of our approach precludes us from examining the complicated dynamics of the collision itself (cf. Johnson et al. 2015; Wakita et al. 2017; Davies et al. 2020). However, it does allow us to describe, broadly and intuitively, the simpler post-collision evolution of the silicate cloud, and to economically survey the range of possible outcomes. We will make use of our model’s flexibility to scale results to proto-Kuiper belt conditions, to see if we might reproduce the chondrule-like thermal histories inferred from cometary samples returned by the *Stardust* mission (Nakamura et al. 2008; Jacob et al. 2009; Bridges et al. 2012; Brownlee 2014; Gainsforth et al. 2015). Our approach complements that of Stewart et al. (2019a), who present an ab initio simulation of a vaporizing collision in substantive detail.

The rest of this paper is organized as follows. In section 2 we describe our model of chondrule formation using a fiducial set of initial vapor cloud parameters in the main asteroid belt of the solar nebula. In section 3 we explore how our results vary over the space of initial cloud properties (density, temperature, size) and protoplanetary disc conditions, including those that might have characterized the proto-Kuiper belt. A summary and outlook are given in section 4.

2 CHONDRULE FORMATION MODEL

We start our analysis at a time post-collision when a cloud of hot silicate vapor is expanding into the ambient hydrogen nebula. The cloud is dominated by vapor but contains solid ejecta of various sizes, among which are chondrule precursors. Some fraction of the original colliding pair of planetesimals is assumed to remain in a gravitationally bound mass at the center of the cloud; we will refer to the remnant mass as the disrupted “parent body” or “planetesimal”. The vapor cloud is assumed spherical and sufficiently decompressed that it behaves as an ideal gas; we do not model the prior non-ideal phase of the explosion (cf. Johnson et al. 2015; Stewart et al. 2019a; Davies et al. 2020).

Our fiducial input parameter values include the vapor cloud’s initial radius $R_0 = 200$ km, initial temperature $T_0 = 4000$ K, and initial mass density $\rho_0 = 10^{-5}$ g/cm³. For

simplicity and to reduce the number of free parameters in the model, the radius of the underlying disrupted planetesimal is assumed to scale with the initial size of the cloud: $R_{\text{pl}} = R_0/2$, and so the planetesimal mass $M = (4\pi/3)\rho_{\text{solid}}(R_0/2)^3$ for $\rho_{\text{solid}} = 3$ g/cm³. Our analysis is restricted to zeroth-order properties of the cloud, e.g. its mean temperature and pressure; for the most part, we will not attempt to spatially resolve the cloud. We stage our calculations at ~ 3 au, where the main asteroid belt resides; we assume the local density of the background hydrogen nebula is $\rho_{\text{neb}} = 10^{-9}$ g/cm³, about 10 times higher than that of the minimum-mass solar nebula (e.g. Chiang & Youdin 2010) and 3 times smaller than the density of a gravitationally unstable (Toomre $Q \sim 1$) disc at this distance.

Sections 2.1–2.3 describe, in chronological order, the dynamical and thermal evolution of the cloud. Section 2.4 considers the evolution of a proto-chondrule, treated as a kind of test particle in the cloud. Different parameter choices are explored in section 3.

2.1 Overpressured expansion and adiabatic cooling

At the start of our calculation (time $t = 0$), the cloud pressure greatly exceeds the nebular pressure, and the nebular mass displaced by the cloud is small compared to the cloud mass; thus the cloud expands nearly freely. We assume the expansion velocity u at this time is at its peak value, $u = \max u = u_0$, and is such that the cloud’s bulk kinetic energy per unit mass, $(1/2)u_0^2$, is comparable to its internal energy $kT_0/[(\gamma - 1)\mu m_p]$ (Zel’dovich & Raizer 1967):

$$u_0 \sim \left(\frac{2kT_0}{(\gamma - 1)\mu m_p} \right)^{1/2} \\ \sim 2.6 \text{ km s}^{-1} \left(\frac{T_0}{4000 \text{ K}} \right)^{1/2} \quad (1)$$

where k is Boltzmann’s constant, m_p is the proton mass, and $\mu = 30$ and $\gamma = 4/3$ (Melosh 1989) are the mean molecular weight and adiabatic index, respectively, of hot silicate vapor, mostly comprising SiO, Na, O, and O₂ (e.g. figure 4 of Fegley & Schaefer 2012) whose molecular ro-vibrational degrees of freedom are excited. In reality u_0 may be somewhat higher than given by (1) because the expansion speed at $t = 0$ respects how much thermal energy is present during the cloud’s inception at $t < 0$, when the temperature may exceed T_0 . We neglect this order-unity correction, which is also complicated by non-ideal-gas effects.

The cloud’s initial expansion is supersonic with respect to the surrounding nebula. For a nebular temperature at 3 au of 75 K (unheated by the explosion) and a mean molecular weight of $\mu_{\text{neb}} = 2.4$ for solar composition gas, the nebular sound speed is $c_{\text{neb}} = 0.5$ km/s and $u_0/c_{\text{neb}} = 5$. The forward shock sweeps nebular gas into a shell surrounding the cloud, slowing its expansion. By the time the cloud has grown to radius R , its velocity has decreased to

$$u(R) = \dot{R}(R) = \frac{u_0}{1 + (\rho_{\text{neb}}/\rho_0)(R/R_0)^3} \quad (2)$$

if we assume momentum conservation (as opposed to energy conservation, which breaks down from radiative losses that

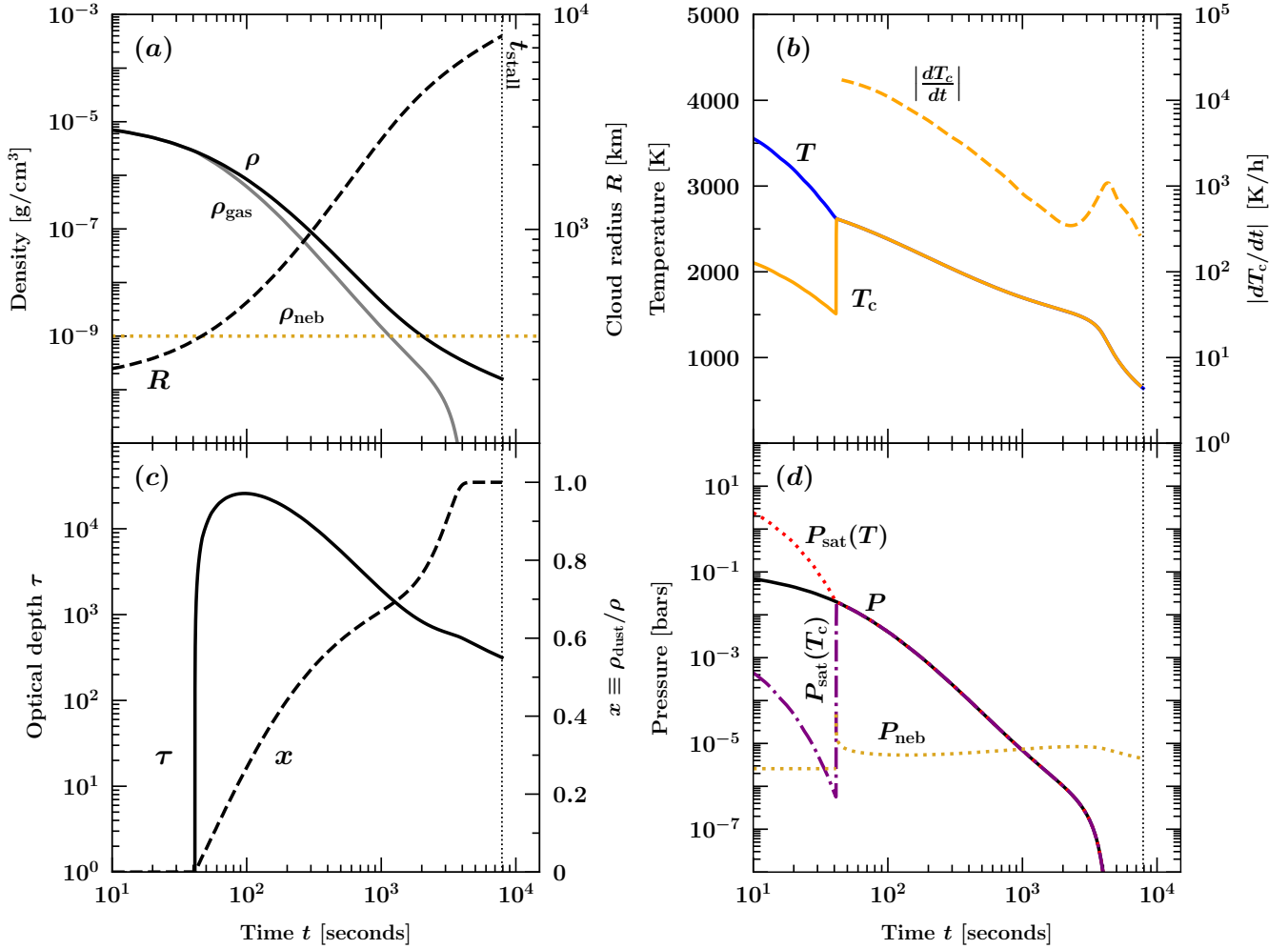


Figure 1. Evolution of the silicate vapor cloud and an embedded chondrule precursor of radius $s_c = 0.3$ mm. The cloud expands freely at first ($R \propto t$, panel a). Later the cloud slows in the snow-plough phase because of nebular mass loading ($R \propto t^{1/4}$ asymptotically). The cloud total density ρ scales as $1/R^3$ (panel a). The cloud temperature T and pressure P initially fall adiabatically (panels b and d), while the proto-chondrule is heated conductively by the silicate vapor and cools by blackbody emission to reach an equilibrium temperature $T_c < T$ (panel b). The chondrule precursor does not vaporize because its saturation vapor pressure $P_{\text{sat}}(T_c) < P$ (panel d). At $t \sim 40$ s, the cloud saturates and vapor starts to condense into dust of mass fraction $x = \rho_{\text{dust}}/\rho$ (panel c); the gas density ρ_{gas} is now less than ρ (panel a). Once saturated, the cloud stays saturated with $P = P_{\text{sat}}(T)$, and for a time, T falls more slowly than along the original adiabat because of latent heat release. The nebular pressure P_{neb} just outside the cloud is higher than before dust condensation because of heating by dust-emitted radiation. The dust optical depth τ is always $\gg 1$ (panel c) but by $t \sim 3000$ s has decreased enough that radiative cooling causes T to drop faster, all of the remaining vapor to condense ($x = 1$), and P to nosedive. Radiative heating by dust enforces $T_c = T$; the chondrule cools with the cloud over a few hours (see also dT_c/dt in panel b). We end our calculation at $t_{\text{stall}} \sim 8000$ s (vertical dotted line) when the external nebular pressure has brought the cloud to a halt and nebular gas starts to backfill the pressure-less cavity left by condensation.

we will describe in section 2.3). Equation (2) can be solved for $R(t)$, from which the cloud’s mean density

$$\rho(t) = \rho_0 \left(\frac{R_0}{R(t)} \right)^3 \quad (3)$$

follows. Fig. 1a shows $R(t)$ (dashed black curve) and $\rho(t)$ (solid black curve) for our fiducial parameters. For $t \lesssim 2 \times 10^3$ s, the cloud expands at near-constant velocity $u \approx u_0$ so that $R \propto t$ and $\rho \propto t^{-3}$. For $t \gtrsim 2 \times 10^3$ s, the swept-up nebular mass becomes comparable to the silicate cloud mass and the expansion slows, with $R(t)$ and $\rho(t)$ approaching their asymptotic $t^{1/4}$ and $t^{-3/4}$ scalings, respectively. The cloud

at this stage is said to be in a momentum-conserving “snow-plough” phase (e.g. Shu 1992).

Initially, as the cloud expands, its mean temperature and pressure drop adiabatically from their starting values T_0 and $P_0 = \rho_0 k T_0 / (\mu m_p)$:

$$\frac{T}{T_0} = \left(\frac{\rho}{\rho_0} \right)^{\gamma-1} \quad (4)$$

$$\frac{P}{P_0} = \left(\frac{\rho}{\rho_0} \right)^{\gamma} \quad (5)$$

with $\gamma = 4/3$ as stated earlier. These relations describe the

silicate cloud material, not the piled-up nebular mass. Fig. 1 shows $T(t)$ (panel b) and $P(t)$ (panel d).

2.2 Condensation

The silicate vapor departs from the original adiabat at $t \sim 40$ s, when it cools sufficiently that it starts to re-condense into liquid/solid droplets (hereafter “dust”—not to be confused with chondrules, which will not be discussed until section 2.4). Condensation occurs when the saturation vapor pressure P_{sat} given by

$$\log_{10} \left(\frac{P_{\text{sat}}}{\text{bars}} \right) = -30.6757 - \frac{8228.146 \text{ K}}{T} + 9.3974 \log_{10} \left(\frac{T}{\text{K}} \right) \quad (6)$$

falls below the cloud pressure P . We use here the vapor pressure for molten bulk silicate Earth (“BSE”), whose chemical composition is similar to that of olivine-rich chondrites (Fegley & Schaefer 2012). Once saturated, the cloud remains saturated, with the gas pressure P equal to $P_{\text{sat}}(T)$ (Zel’dovich & Raizer 1967; Melosh 1989).¹

Condensation releases latent heat, which keeps the gas warmer than it would be along the original adiabat. The temperature of the dust-gas mixture evolves from adiabatic cooling, release of latent heat, and radiation emitted by dust:

$$\frac{4\pi\rho R^3}{3} \left([C_{\text{gas}}(1-x) + C_{\text{solid}}x] dT - \frac{k}{\mu m_{\text{p}}} T(1-x) \frac{d\rho}{\rho} - [L_{\text{vap}} - (C_{\text{solid}} - C_{\text{gas}})T] dx \right) = -\frac{4\pi R^2 \sigma_{\text{SB}} T^4}{\tau} dt. \quad (7)$$

The left-hand side of (7) is taken from Zel’dovich & Raizer (1967, chapter 8), where $x \equiv \rho_{\text{dust}}/\rho$ is the mass fraction in condensates, $C_{\text{gas}} = 6.3 \times 10^6$ erg/(g K) is the gas specific heat at constant volume (Melosh 1989), $C_{\text{solid}} = 10^7$ erg/(g K) is the specific heat of dust, and $L_{\text{vap}} = 3 \times 10^{10}$ erg/g is the heat of silicate vaporization (measured for pure forsterite; Nagahara et al. 1994). Whereas Zel’dovich & Raizer (1967) have no right-hand side term because they assume strict energy conservation, we account in our right-hand side for thermal photons that diffuse out of the assumed optically thick cloud, with σ_{SB} equal to the Stefan-Boltzmann constant and

$$\tau = \frac{3\rho R}{4\rho_{\text{solid}} s_{\text{dust}}} x \quad (8)$$

equal to the cloud radial optical depth, assuming that vapor condenses into dust grains of radius s_{dust} and internal density ρ_{solid} that present geometric cross section to photons. Our radiative loss term in (7) presumes that the cloud is in radiative equilibrium, with the bulk of the dust at temperature T heating photospheric dust near the cloud outer boundary to a temperature of $\sim T/\tau^{1/4}$. We take $s_{\text{dust}} = 1 \mu\text{m}$, comparable in size to vapor condensates in other settings, including terrestrial experiments of condensing silicate and metal vapor (Melosh 1989, page 70), silicate clouds in exoplanet atmospheres (e.g. Gao et al. 2020), and vapor plumes of meteors

¹ The cloud may super-cool along the original adiabat before equilibrium condensation sets in. For our cloud whose expansion speed does not greatly exceed the thermal speed of its constituent gas molecules, and which may be full of impurities and condensation sites (i.e., liquid/solid ejecta from the original collision), this departure from equilibrium should be brief.

impacting the Earth at $\lesssim 15$ km/s (Johnson & Melosh 2012, their figure 13). We test different values of s_{dust} in section 3.

Equation (7) is solved numerically for $T(t)$ and $x(t)$, in conjunction with Eqs. (2) and (3) for $R(t)$ and $\rho(t)$, and the condition $P = (1-x)\rho kT/(\mu m_{\text{p}}) = P_{\text{sat}}(T)$. Fig. 1 shows how, after $t \sim 40$ s, our fiducial cloud cools sufficiently that $P_{\text{sat}}(T)$ crosses and subsequently locks to P (panel d); an order-unity fraction of the cloud mass condenses into dust and renders the cloud optically thick (panel b); and the cloud temperature drops more slowly with time than it did along the original adiabat because of latent heat release (panel c). We have verified that the cloud is in radiative equilibrium insofar as the photon diffusion time $\tau R/c$, where c is the speed of light, is either comparable to or less than the elapsed time t . We have also checked that gas and dust conduct heat to one another so efficiently (via gas-dust collisions) that both species are at very nearly the same temperature at any given time.

2.3 Radiative losses and nebular backfilling

Eventually, as the cloud expands and becomes less optically thick, an order-unity fraction of the cloud’s thermal energy is lost to radiation. From Fig. 1b, we see that radiative losses become significant at $t \sim 3000$ s. This is also around the time when nebular mass loading slows the expansion velocity by a factor of ~ 2 and the cloud enters the snow-plough phase (section 2.1). After this time, T declines faster than before, scaling approximately as $s_{\text{dust}}^{-1/3} t^{-2/3}$; this can be seen from equation 7 by ignoring the volume expansion and latent heat terms, and using $R \propto t^{1/4}$ (equation 2 in the snow-plough phase) and constant $x \sim 1$. The faster temperature drop leads residual silicate vapor to further condense, and the gas density plummets (Fig. 1a).

Thus radiation losses and condensation cause the internal cloud pressure to fall dramatically below the external nebular pressure (Fig. 1d). The resulting adverse pressure gradient further slows the cloud’s expansion and ultimately halts it. We estimate the time for the cloud to stall using the following order-of-magnitude argument. If we assume a fluid parcel near the cloud-nebula interface has a total density $\rho + \rho_{\text{neb}}$, then the local pressure gradient $-\nabla P$ slows the parcel down from its velocity u over a timescale

$$\begin{aligned} t_{\text{stall}} &\sim \frac{u}{|\nabla P|/(\rho + \rho_{\text{neb}})} \\ &\sim \frac{u(\rho + \rho_{\text{neb}})R}{P_{\text{neb}} - P} \end{aligned} \quad (9)$$

where we have estimated that the pressure changes over a length scale $\sim R$. Because the cloud’s motion during this late stage is not strongly supersonic, the swept-up nebular mass should not be highly compressed, i.e., the cloud boundary should not be sharp. We solve numerically for the time $t = t_{\text{stall}}$ when the right-hand side of (9) (evaluated as a running quantity with time) equals the time elapsed. The nebular pressure P_{neb} is evaluated using the background nebular density ρ_{neb} and a temperature $T_{\text{neb}} = T/\tau^{1/4}$, which accounts approximately for radiative heating by the underlying cloud.

For our fiducial parameters, $t_{\text{stall}} \sim 8000$ seconds, at which time the cloud, now almost fully condensed into dust,

has radiatively cooled down to $T \sim 600$ K. We stop our calculation of the cloud evolution at t_{stall} . After this time, nebular gas backfills the near pressure-less cavity left by condensation. Insofar as the cavity will not be perfectly spherically symmetric, the backfilling will be chaotic, with streams of nebular gas crossing each other at near-sonic speeds on the way in, producing mild shocks, hydrodynamic instabilities, and turbulence (cf. [Stewart et al. 2019a](#)). Cloud dust that mixes with nebular gas will be quenched by conduction down to $\mathcal{O}(10^2$ K). The backfilling should take on the order of the nebular sound-crossing time of the cavity, $\mathcal{O}(10^4$ s).

2.4 Chondrules

Having described in the preceding sections 2.1–2.3 the evolution of the silicate cloud, we now examine how chondrules may be created within such a cloud.

We assume at $t = 0$ that the cloud, of size R_0 , contains chondrule precursor solids, modeled as spheres of internal density ρ_{solid} and radius s_c , ejected from the originating collision. It is not obvious that chondrule-sized solids survive the “fireball” at $t < 0$, when $R < R_0$, $T > T_0$, and $\rho > \rho_0$; solids vaporize if they are too small and exposed to hot vapor for too long. As we do not model the complicated collision and cloud dynamics at $t < 0$, we cannot say what small solids are present by the time the cloud has grown to size R_0 . Nevertheless, it seems plausible that the cloud at this moment is filled with debris of various sizes. The collisional destruction of the target planetesimal is not instantaneous, but unfolds over the finite interval of time it takes the impactor to finish smashing into the target. For a collision between similarly sized bodies, this time is comparable to the time for the vapor cloud to grow to size R_0 , as the planetesimal sizes and R_0 are comparable (by construction), and the vapor expansion velocity is comparable to the impactor-target relative velocity (see section 1 and equation 1). During this “smash-through” phase, which lasts $\mathcal{O}(1$ min) for our fiducial parameters, solid debris of all sizes should be continuously generated by the collision. While mm-sized debris released when the impactor first makes contact with the target may not last to $t = 0$, particles released towards the end of the smash-through phase, just before $t = 0$, may survive. In the following subsections we consider how the solid/liquid debris that survives may be processed into the chondrules we observe today.

The expanding cloud drags with it particles smaller than a certain size. Those particles of mass m_c whose aerodynamic stopping times

$$t_{\text{stop}} = \frac{m_c u}{F_{\text{drag}}} \quad (10)$$

are less than the dynamical time R/u are swept along at speed u . At the earliest times, the drag force $F_{\text{drag}} \sim \rho u^2 \pi s_c^2$, as appropriate for moderately high Reynolds number flow around an obstacle (e.g. [Weidenschilling 1977](#), their equation 8). Evaluating the condition $t_{\text{stop}} < R/u$ at $t = 0$ implies that $s_c \lesssim 60$ cm sized particles are entrained with the cloud. We will see in section 2.4.2 how this size range dramatically narrows for particles that fall back to the disrupted parent body. Of course the total amount of solid mass entrained by the cloud cannot exceed the cloud’s mass.

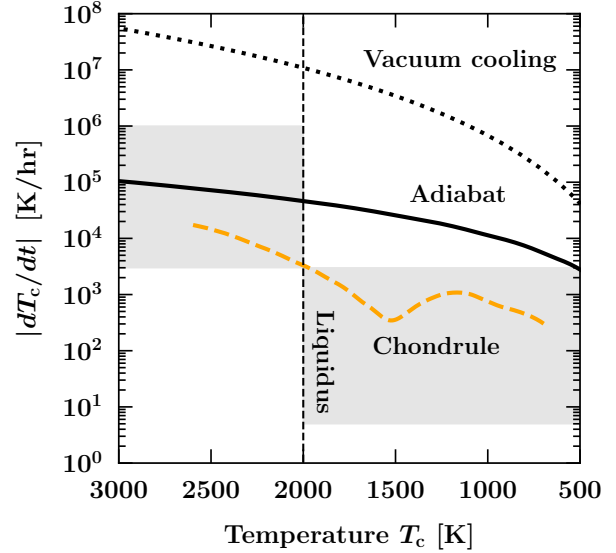


Figure 2. Chondrule cooling rate vs. temperature (dashed orange curve), shown from the point the cloud saturates (in this regime radiation by newly condensed dust enforces $T_c = T$, and T_c falls monotonically). From $T_c = 2500$ K down to $T_c = 1500$ K, cooling is mostly driven by the cloud’s expansion, with cooling rates lower than given by the original adiabat (solid curve) which does not account for latent heat released by condensation. Also shown for comparison is the blackbody cooling rate in vacuum ($dT_c/dt = 4\pi s_c^2 \sigma_{\text{SB}} T_c^4 / (m_c C_{\text{solid}})$; dotted curve). For $T_c \lesssim 1500$ K, radiative losses from the cloud as a whole become important and the cooling rate increases. The shaded regions highlight super and sub-liquidus cooling rates inferred from laboratory experiments. These constraints are taken from [Desch & Connolly \(2002\)](#), except for the poorly constrained upper bound to the super-liquidus cooling rate which we arbitrarily set at 10^6 K/hr.

2.4.1 Thermal history

Proto-chondrules exchange heat with their environment by gas conduction and radiation. Their temperature T_c evolves as:

$$\frac{4\pi}{3} s_c^3 \rho_{\text{solid}} C_{\text{solid}} \frac{dT_c}{dt} = n_{\text{gas}} \pi s_c^2 u_{\text{th}} k (T - T_c) + 4\pi s_c^2 \sigma_{\text{SB}} (T^4 - T_c^4) \quad (11)$$

where $n_{\text{gas}} = (1 - x)\rho / (\mu m_p)$ is the number density of gas molecules, $u_{\text{th}} = \sqrt{8kT / (\pi \mu m_p)}$ is the gas mean thermal speed, and each collision between a gas molecule and a chondrule is assumed to transfer an energy $k(T - T_c)$. The heating term proportional to $\sigma_{\text{SB}} T^4$ is due to the background radiation field emitted by optically thick dust (after it condenses). What equation (11) omits is drag-heating by the silicate vapor, but this effect lasts only briefly, for the fraction of a second it takes the chondrule to come up to speed with the cloud, and even then adds only marginally to conductive heating.

Equation (11) is solved for $T_c(t)$, with the background variables $n_{\text{gas}}(t)$ and $T(t)$ calculated separately as described in previous sections. We choose a fiducial chondrule radius of $s_c = 0.3$ mm—sizes of this order will be justified in section 2.4.2 when we discuss the aerodynamics of re-agglomeration—and assume a temperature at $t = 0$ of $T_c(0) = 10^3$ K. This initial temperature, which is merely an order-of-magnitude guess because we do not model the fireball dynamics at $t < 0$, is quickly forgotten as the proto-chondrule comes into dynamical and thermal equilibrium with its environment.

Fig. 1b shows $T_c(t)$. Initially, conductive heating is balanced by radiative cooling into the optically thin cloud (dust has not yet condensed), and the chondrule is at a temperature of $T_c \sim 2000$ K. The saturation vapor pressure of the chondrule, $P_{\text{sat}}(T_c)$ (equation 6), sits a factor of > 100 below the ambient gas pressure P (Fig. 1d), safeguarding the chondrule against vaporization (for a study of the time-dependent kinetics of vaporization and volatile retention, see Dullemond et al. 2016). Over the next ~ 30 s, the chondrule remains colder than, but cools in lockstep with, the adiabatically expanding background gas, falling to $T_c \sim 1500$ K. At $t \sim 40$ s, the chondrule heats back up to ~ 2600 K when dust condenses and renders the entire cloud optically thick — the chondrule is literally “flash-heated” by the radiation emitted by newly condensed dust. The chondrule is now trapped in this radiation bath and $T_c \simeq T$. Over the course of ~ 5 minutes, the temperature falls from ~ 2600 K through the liquidus of ~ 2000 K; it then passes through the solidus, here estimated to be ~ 1500 K, after ~ 30 minutes. Cooling rates $|dT_c/dt|$ are plotted versus t in Fig. 1b and versus T_c in Fig. 2. Above the liquidus, $|dT_c/dt| \sim 3000\text{--}20000$ K/hr, while below the liquidus $|dT_c/dt| \sim 300\text{--}3000$ K/hr. These cooling rates appear compatible with empirically determined chondrule cooling rates (e.g. Desch & Connolly 2002; Connolly Jr. & Jones 2016), shown as grey regions in Fig. 2. This figure also shows that adiabatic cooling alone predicts cooling rates that exceed sub-liquidus experimental rates by at least an order of magnitude; cooling buffered by dust condensation is essential to reproducing chondrule cooling rates.

2.4.2 Re-agglomeration and size sorting

During the initially highly over-pressured, free-expansion phase of the explosion, particles less than about a meter in size are dragged outward by the expanding silicate cloud (see equation 10 and surrounding discussion). Together, particles and vapor follow a Hubble-like velocity profile, with velocity increasing linearly with radius up to the cloud boundary velocity of u_0 (e.g. Chevalier & Fransson 2017).

The situation changes as the cloud stalls against the pressure of the external nebula. Condensation leaves a cavity that nebular gas begins to backfill. The cavity at this stage has radius $R_{\text{stall}} \sim 10^4$ km (Fig. 1a); filling it back in and restoring pressure equilibrium mobilizes nebular gas on a similar scale R_{stall} (see discussion below equation 9). To determine which particles are swept inward by this backfilling nebular gas and which continue to sail out (see also Lock et al. 2019), we idealize the inflowing gas as a slab of thickness R_{stall} moving inward at the nebular sound speed $c_{\text{neb}} = \sqrt{kT_{\text{neb}}/(\mu_{\text{neb}}m_p)}$, and imagine the chondrules encountering this column with an initial outward velocity of $u_0/2$. Each chondrule feels a nebular drag force

$$F_{\text{drag}} = \frac{4\pi}{3} \rho_{\text{neb}} s_c^2 u_{\text{th}} u_{\text{rel}}, \quad (12)$$

evaluated in the free-molecular limit where the gas collisional mean free path exceeds the chondrule radius s_c (Epstein 1924). Here the mean thermal velocity $u_{\text{th}} = \sqrt{8kT_{\text{neb}}/\pi\mu_{\text{neb}}m_p}$, and the chondrule-gas relative velocity $u_{\text{rel}} = u_0/2 + c_{\text{neb}}$. For a chondrule of mass m_c to reverse

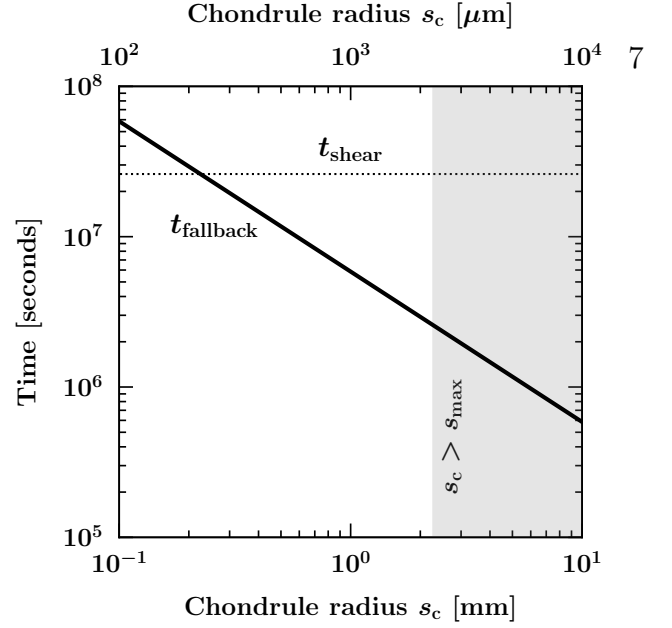


Figure 3. The size range of solids that initially expand outward with the cloud but ultimately turn around to re-agglomerate onto the parent planetesimal. When nebular gas backfills the cavity created by condensation, it drags inward solids with radii $s_c < s_{\text{max}}$; solids that are larger fail to be aerodynamically stopped and are lost to space. Smaller particles gravitationally settle toward the parent body in a time $t_{\text{fallback}} \propto s_c^{-1}$. They successfully land onto the parent if t_{fallback} is less than t_{shear} , the time for material surrounding the planetesimal to be shorn away by solar tidal forces. The constraints $s_c < s_{\text{max}}$ and $t_{\text{fallback}} < t_{\text{shear}}$ are satisfied for $0.2 \text{ mm} \lesssim s_c \lesssim 2 \text{ mm}$, similar to the measured sizes of chondrules.

direction, it must be dragged to a stop over a time

$$\Delta t_{\text{stop}} \sim \frac{m_c u_{\text{rel}}}{F_{\text{drag}}} \sim \frac{\rho_{\text{solid}} s_c}{\rho_{\text{neb}} u_{\text{th}}} \quad (13)$$

that is shorter than the time the chondrule takes to cross and exit the slab

$$\Delta t_{\text{cross}} \sim \frac{R_{\text{stall}}}{u_0/2 + c_{\text{neb}}}. \quad (14)$$

The condition $\Delta t_{\text{stop}} < \Delta t_{\text{cross}}$ implies that only chondrules of radius

$$s_c < s_{\text{max}} \sim \frac{\rho_{\text{neb}}}{\rho_{\text{solid}}} \frac{u_{\text{th}}}{c_{\text{neb}} + u_0/2} R_{\text{stall}} \sim 2.6 \text{ mm} \left(\frac{R_{\text{stall}}}{10^4 \text{ km}} \right) \left(\frac{\rho_{\text{neb}}}{10^{-9} \text{ g/cm}^3} \right) \quad (15)$$

are swept back into the cavity. Much larger particles have too much inertia and sail out to distances $\gg R_{\text{stall}}$ where the nebula is unaffected by the explosion.

The backfilling of the cavity by nebular gas does not by itself bring $s_c < s_{\text{max}}$ sized particles all the way back to the cavity center where the disrupted planetesimal resides. As described at the end of section 2.3, gas inflows will be asymmetric and not completely radial, and will not directly reach the origin. Particles swept in by these flows will be stopped by collisions between gas streams, at radial distances not much smaller than R_{stall} . The particles will be buffeted by turbulence in the nebular hydrogen that re-fills the cavity.

Nevertheless such turbulence, absent driving, eventually decays away. Random motions subside over a cloud sound-crossing time of $\mathcal{O}(10^4 \text{ s})$, after which embedded particles gravitationally settle through the hydrogen cloud toward the disrupted planetesimal. Starting at a radial distance r_{init} ,

and falling at a drag-limited terminal velocity $(GM/r^2)\Delta t_{\text{stop}}$, where $M = (4\pi/3)\rho_{\text{solid}}(R_0/2)^3$ is the planetesimal mass, particles rain back down onto the parent body in a time

$$t_{\text{fallback}} \approx \frac{r_{\text{init}}^3}{3GM} \frac{u_{\text{th}}}{s_c} \frac{\rho_{\text{neb}}}{\rho_{\text{solid}}}. \quad (16)$$

Particles that are too small do not make it back, as their fallback times exceed

$$t_{\text{shear}} \sim \left(\frac{GM_{\odot}}{a^3}\right)^{-1/2} \sim 2.6 \times 10^7 \text{ seconds} \left(\frac{a}{3 \text{ au}}\right)^{3/2}, \quad (17)$$

the timescale for solar tidal forces to shear the cloud apart at heliocentric distance a . The condition $t_{\text{fallback}} < t_{\text{shear}}$ sets the minimum radius particle that can re-agglomerate with its parent; smaller particles cannot sediment fast enough before they are tidally shorn away. Fig. 3 compares t_{shear} and t_{fallback} as a function of particle size for $r_{\text{init}} = R_{\text{stall}}/3$, and shows that this minimum particle radius is

$$s_{\text{min}} \sim \frac{(R_{\text{stall}}/3)^3}{3GM} \frac{u_{\text{th}}}{t_{\text{shear}}} \frac{\rho_{\text{neb}}}{\rho_{\text{solid}}} \sim 0.2 \text{ mm} \quad (18)$$

for our fiducial parameters. We see that s_{min} and s_{max} bracket a range of particle sizes similar to the range of sizes exhibited by chondrules (see Friedrich et al. 2015 for empirical data), modulo the sensitivity of s_{min} to the uncertain order-unity factor relating r_{init} to R_{stall} .

What happens to all of the dust which condenses out of the silicate vapor? Most of it will be torn by solar tides away from the remains of the parent body and dispersed into the protoplanetary disc. Some of it may be reincorporated into the planetesimal. The dust that is closest to the parent may settle back down onto its surface to form chondritic matrix. Other dust grains may be accreted by chondrules to form their fine-grained rims (e.g. Huss et al. 1981). Krot & Wasson (1995) have noted the petrologic similarity between matrix and chondrule rims.

3 HOW CHONDRULE PROPERTIES VARY WITH VAPOR CLOUD AND NEBULAR PROPERTIES

We explore how model outcomes change with initial cloud properties ρ_0 , R_0 , and T_0 , as well as the sizes of condensed dust grains s_{dust} and the background nebular density ρ_{neb} . Unless otherwise indicated, we vary one parameter at a time while holding others fixed at their fiducial values $(\rho_0, R_0, T_0, \rho_{\text{neb}}, s_{\text{dust}}) = (10^{-5} \text{ g/cm}^3, 200 \text{ km}, 4000 \text{ K}, 10^{-9} \text{ g/cm}^3, 1 \mu\text{m})$. Section 3.1 examines how cooling rates vary over parameter space, section 3.2 studies how the size distribution of chondrules varies, and section 3.3 scales our model to conditions in the outer Solar System where Kuiper belt objects may have formed, near ~ 15 au.

3.1 Variations in cooling rates

Figs. 4 and 5 show how chondrule cooling rates dT_c/dt depend on cloud initial conditions. Cooling rates are plotted

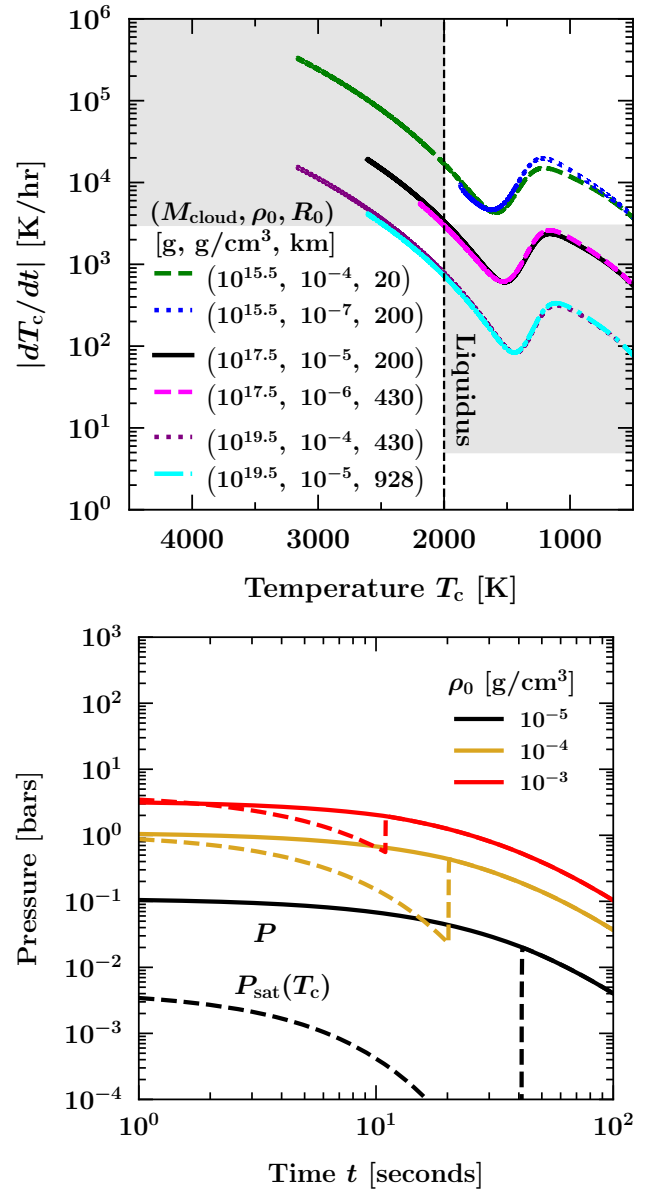


Figure 4. *Top:* Chondrule cooling rates vs. temperature (as in Fig. 2) for various initial cloud densities ρ_0 and radii R_0 . Cooling rates scale with the total mass of the cloud, $dT_c/dt \propto M_{\text{cloud}}^{-1/3}$ (equation 19), where $M_{\text{cloud}} \sim \rho_0 R_0^3$. Cooling rates satisfy experimental constraints (shaded regions) for $M_{\text{cloud}} \gtrsim 10^{17}$ g. *Bottom:* Chondrule vapor pressure $P_{\text{sat}}(T_c)$ compared against the ambient gas pressure P for different initial cloud densities. When $\rho_0 \gtrsim 10^{-3}$ g/cm³, conductive heating within the first minute is so strong that $P_{\text{sat}}(T_c) > P$ and the chondrule vaporizes. The upper bound on ρ_0 , together with the lower bound on M_{cloud} , require $R_0 \gtrsim 30$ km, corresponding to a parent planetesimal radius $R_{\text{pl}} = R_0/2 \gtrsim 15$ km.

when vapor saturates, dust forms, and the chondrule temperature T_c , radiatively locked to the cloud temperature T , falls monotonically (see Figure 2).

Fig. 4a varies the cloud's initial radius R_0 and initial density ρ_0 , and demonstrates that what matters for the cooling rate dT_c/dt at a given temperature T is the product $\rho_0 R_0^3$,

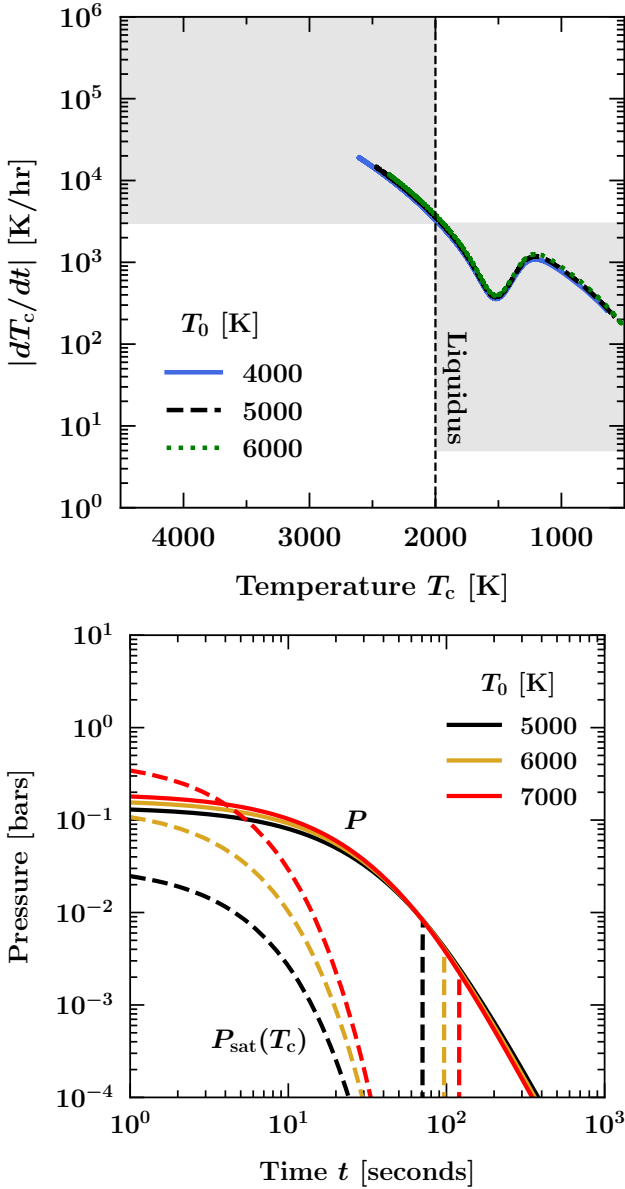


Figure 5. Same as Fig. 4, but for different initial cloud temperatures T_0 . The value of T_0 has little effect on cooling rates (top panel) because cooling is governed by the equilibrium condition $P = P_{\text{sat}}(T)$ which is independent of initial conditions. Nevertheless, T_0 cannot be too high or else the chondrule vaporizes at early times before the cloud saturates (bottom panel). For our fiducial $\rho_0 = 10^{-5} \text{ g/cm}^3$, the chondrule vaporizes when $T_0 \gtrsim 7000 \text{ K}$.

i.e., the total cloud mass $M_{\text{cloud}} (= 4\pi\rho_0 R_0^3/3$, multiplied by 7/8 to account for the volume occupied by the underlying planetesimal). This dependence follows from

$$\frac{dT_c}{dt} = \frac{dT}{dt} = \frac{dT}{d\rho} \frac{d\rho}{dR} \frac{dR}{dt}. \quad (19)$$

The factor $dT/d\rho$ depends only the equilibrium thermodynamics of adiabatic cooling and condensation, which specifies $\rho(T)$ (equation 7), and does not depend on the initial conditions ρ_0 or R_0 . The second factor $d\rho/dR \propto \rho/R$ (equation 3), which for given $\rho(T)$ scales as $1/R \propto M_{\text{cloud}}^{-1/3}$. The final fac-

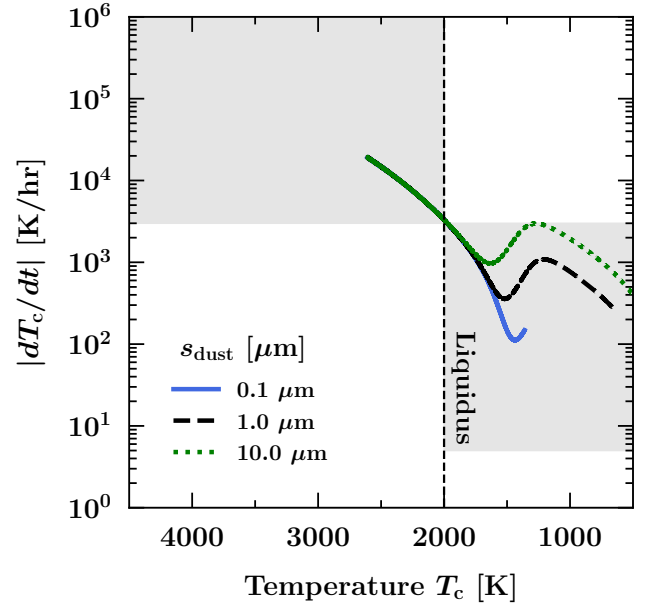


Figure 6. Cooling rates vs. temperature for different assumed radii s_{dust} of condensed dust particles. The dust size does not matter at higher temperatures (early times) when the cloud cools by expanding and loses negligible energy to radiation. Larger dust grains render the cloud less optically thick and hasten the onset of radiative losses, which increase cooling rates.

tor dR/dt is constant ($= u_0$) during the free-expansion phase, and depends only on $\rho_0 R_0^3/R^3 \propto \rho(T)$ during the snow-plough phase (equation 2). Putting it all together, we see that dT_c/dt scales as $M_{\text{cloud}}^{-1/3}$ at all times; a more massive cloud cools more slowly because to reach a given $\rho(T)$ it needs to expand to a larger radius R , when its dynamical time R/\dot{R} is longer. According to Fig. 4a, cloud masses $M_{\text{cloud}} \gtrsim 10^{17} \text{ g}$ yield chondrule sub-liquidus cooling rates consistent with those measured in the lab.

Chondrules are heated by conduction with gas. The higher are ρ_0 and T_0 , the higher are chondrule peak temperatures. Too high a T_c causes the chondrule vapor pressure $P_{\text{sat}}(T_c)$ to exceed the ambient cloud pressure P , at which point the chondrule vaporizes (see Dullemond et al. 2016 for a treatment of evaporation/condensation kinetics). To keep chondrule precursors intact, the initial cloud density ρ_0 must be $\lesssim 10^{-3} \text{ g/cm}^3$ (Fig. 4b) and the initial cloud temperature T_0 must be $\lesssim 7000 \text{ K}$ (Fig. 5b). The upper bound on ρ_0 , together with the lower bound of 10^{17} g on M_{cloud} (Fig. 4a), imply $R_0 \gtrsim 30 \text{ km}$, which in turn implies the radius of the remnant planetesimal $R_{\text{pl}} = R_0/2 \gtrsim 15 \text{ km}$. The value of T_0 does not much affect the cooling rate post-saturation (Fig. 5a), when $P = P_{\text{sat}}(T)$ and the cloud thermodynamics evolves in an equilibrium fashion with initial conditions largely forgotten. What small differences can be seen in Fig. 5a for dT_c/dt arise from variations in the free-expansion cloud velocity $u_0 \propto T_0^{1/2}$ (equation 1).

Fig. 6 varies s_{dust} , the assumed radii of dust grains that condense out of the silicate vapor. At early times, when cooling is driven by expansion and not radiation, s_{dust} is irrelevant. Radiation becomes important sooner, and cools the cloud faster, for larger s_{dust} which makes the cloud less op-

tically thick (equation 8). Roughly the radiation-dominated cooling rate $dT_c/dt = dT/dt$ at a given T (not t) scales as $s_{\text{dust}}^{1/2}$. This can be seen by using equations 2 (in the snow-plough phase), 3, 7, and 8 to write $dT/dt \propto T^4 R^2 / \tau \propto T^4 s_{\text{dust}} R^4 \propto T^4 s_{\text{dust}} t$, and substituting away t in favor of T using $T \propto s_{\text{dust}}^{-1/3} t^{-2/3}$ (see section 2.2).

3.2 Variations in fallback particle sizes

Panels a-c of Fig. 7 survey a range of initial cloud properties compatible with chondrule thermal histories ($\rho_0 \lesssim 10^{-3} \text{ g/cm}^3$, $R_0 \gtrsim 30 \text{ km}$, $T_0 \lesssim 7000 \text{ K}$; see the preceding subsection), illustrating how these initial conditions affect the sizes of particles that fall back onto the planetesimal (section 2.4.2). In every case plotted, particles on the order of a mm in size fall back and re-agglomerate. The strongest parameter dependencies are seen for s_{min} and its variation with ρ_0 (Fig. 7a), and s_{max} and its variation with R_0 (Fig. 7b). Both trends can be understood simply. If we approximate the size of the cavity left by condensation as $R_{\text{stall}} \sim R_0(\rho_0/\rho_{\text{neb}})^{1/3}$ (technically this is the size of the cloud when it first enters the snow-plough phase, and so is a lower limit on R_{stall}), then equation 15 implies $s_{\text{max}} \propto R_0$, and equation 18 implies $s_{\text{min}} \propto \rho_0$. These scalings agree well with the numerical results in Fig. 7ab. Physically, larger vapor clouds mobilize larger column densities of nebular gas which trap larger particles; and denser clouds stall at larger radial distances where smaller particles cannot gravitationally sediment out before the background shear tears them away.

Fig. 7d indicates that nebular densities ρ_{neb} at 3 au (where we evaluate the tidal disruption time t_{shear}) must be larger than about 10^{-10} g/cm^3 for particles to fall back. If ρ_{neb} is too low, $s_{\text{min}} > s_{\text{max}}$ and no ejected particle of any size can be dragged by nebular gas back toward the planetesimal. The rough scaling arguments used above can be applied here as well to show that $s_{\text{min}} \propto \rho_{\text{neb}}^0$ and $s_{\text{max}} \propto \rho_{\text{neb}}^{2/3}$, trends which are qualitatively confirmed in Fig. 7d. The lower bound on ρ_{neb} is sensitive to our choice for r_{init} , the radial distance from which chondrules fall after nebular gas backfills the cavity and settles down. Throughout this paper for concreteness we have chosen $r_{\text{init}}/R_{\text{stall}} = 1/3$ but this ratio could plausibly be any number between 0.1 and 1. Had we chosen 0.1, s_{min} in Fig. 7d would shift downward by a factor of $\sim 3^3$ (equation 18) and the lower bound on ρ_{neb} would be closer to $10^{-11.5} \text{ g/cm}^3$.

3.3 Collisions in the proto-Kuiper belt

To assess whether collisions can explain the presence of chondrule-like particles collected from the short-period comet 81P/Wild-2 (e.g. Nakamura et al. 2008), we re-scale our model to heliocentric distances possibly appropriate to Wild-2's formation. Short-period comets originate as Kuiper belt objects (KBOs), predominantly of the ‘‘scattered’’ variety having relatively large orbital eccentricities and inclinations (e.g. Nesvorný et al. 2017). Dynamically hot KBOs are thought to reflect a period of upheaval when the orbits of the giant planets (and perhaps those of planets no longer present) underwent large-scale changes driven by gravitational scatterings with remnant planetesimals (e.g. Fernandez & Ip 1984; Malhotra 1995; Tsiganis et al. 2005; Gomes

et al. 2005; Ford & Chiang 2007; Levison et al. 2011; Dawson & Murray-Clay 2012). During this time, Neptune and proto-KBOs were propelled outward from ~ 10 –20 au to 30 au and beyond. Accordingly, we re-stage our calculations for $a = 15 \text{ au}$, near where proto-KBOs may have originated. We adopt a nebular density $\rho_{\text{neb}} = 1.4 \times 10^{-11} \text{ g/cm}^3$, a factor of 70 lower than our fiducial value at 3 au, as follows from the scaling law $\rho_{\text{neb}} \propto a^{-39/14}$ derived for the solar nebula (e.g. Chiang & Youdin 2010). For this orbital distance, the cloud lifetime against tidal forces is $t_{\text{shear}} = 3 \times 10^8 \text{ s} = 10 \text{ yr}$. Additionally, in anticipation of our results for particle re-agglomeration, we set our fiducial chondrule precursor size to $s_c = 10 \mu\text{m}$ when computing chondrule thermal histories $T_c(t)$. All other model parameters are kept at their fiducial values.

Comparison of Fig. 1 with Fig. 8 demonstrates what one might have expected: for a given set of initial cloud conditions (ρ_0 , T_0 , R_0), thermal histories of cloud-embedded particles are qualitatively the same at 3 au as at 15 au. The chondrule thermal evolution is controlled by the internal thermodynamics of the vapor cloud which are not especially sensitive to nebular environment, especially when the cloud is still hot and the chondrule is passing through the liquidus. This is further evidenced in Fig. 9. Sub-liquidus cooling rates dT_c/dt for a given T are marginally faster in the proto-Kuiper belt than in the asteroid belt because the lower nebular density at larger heliocentric distance allows the cloud to expand freely for longer before entering the slower snow-plough phase.

The main effect that lowering the nebular density has is reducing the maximum size of re-agglomerated particles. In the limit of no nebular gas, the maximum size would be zero, as no particle entrained by the supersonically expanding, unbound vapor would ever fall back. As Fig. 10 shows, for our assumed nebular density at 15 au, the maximum radius solid that can be aerodynamically dragged back toward the planetesimal is $s_{\text{max}} = 3 \times 10^{-2} \text{ mm} = 30 \mu\text{m}$, about 60 times smaller than the value at 3 au. The minimum radius s_{min} of fallback particles also decreases, down to about $10 \mu\text{m}$ (10 times smaller than at 3 au), a consequence in part of the longer t_{shear} which allows particles more time to settle. The values of s_{min} and s_{max} would be even smaller if we adopted nebular conditions at $a > 15 \text{ au}$. Thus our model generically predicts that short-period comets and their KBO progenitors should have smaller-sized chondrules compared to chondritic main belt asteroids. This prediction is consistent with the $\sim 10 \mu\text{m}$ sizes of thermally processed solids collected from comet Wild-2, although the possibility remains that the sampled particles are fragments of still larger chondrules. These would be fewer in number following a power-law particle size distribution in the coma. To avoid being disabled by a collision, the *Stardust* spacecraft did not approach close enough to the comet to collect larger particles, and so the concentration of $\gtrsim 100 \mu\text{m}$ chondrules in Wild-2 is unknown.

While we have so far focused on generating chondrule-like particles, comets like Wild-2 are replete with other kinds of equilibrated aggregates (EAs) which were also once partially molten, but which are smaller than chondrules (0.1–1 μm), attained lower peak temperatures ($\sim 1200 \text{ K}$), and skew toward faster cooling rates ($\gtrsim 500 \text{ K/hr}$; Bradley 1994; Brownlee et al. 2005; Messenger et al. 2013). In our

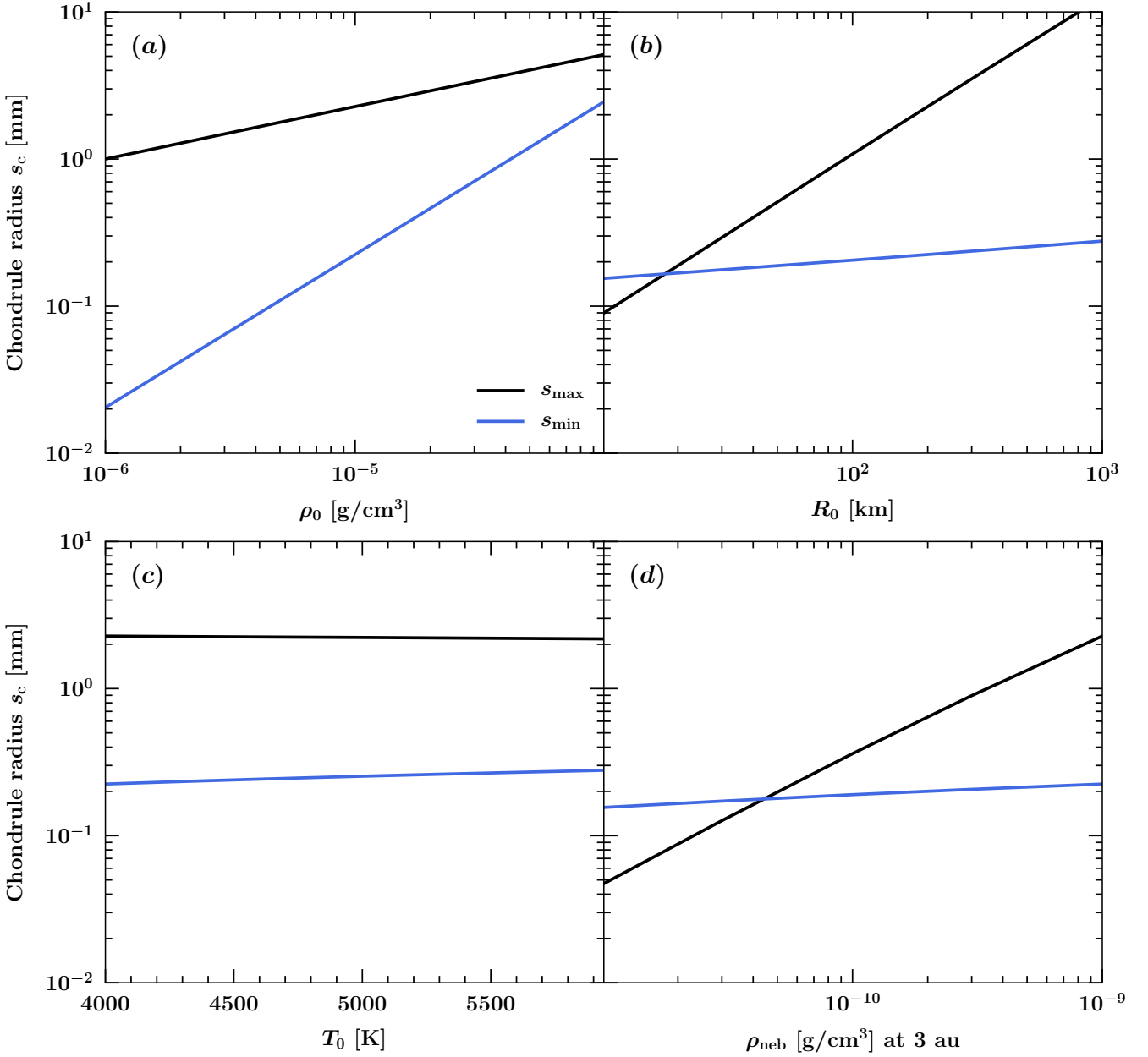


Figure 7. How the size range of re-agglomerated particles depends on cloud initial conditions (panels a-c) and the density of the ambient nebula at 3 au (panel d). For the most part, particle sizes straddling a millimeter result from the same initial cloud conditions that reproduce chondrule thermal histories (see section 3.1). A background nebula with too a low density exerts too little drag on particles and precludes any from re-agglomerating.

model, cooling rates scale inversely with the cloud mass, $dT/dt \propto M_{\text{cloud}}^{-1/3}$, with $M_{\text{cloud}} \gtrsim 10^{17}$ g required to produce the low cooling rates exhibited by chondrules (section 3.1). Lower mass clouds, in the range $M_{\text{cloud}} \sim 10^{15} - 10^{17}$ g, might have hosted the faster cooling EAs; cloud masses and peak temperatures may have been systematically smaller in the proto-Kuiper belt where orbital velocities were slower than in the asteroid belt.

4 SUMMARY AND DISCUSSION

The geologist and pioneering petrographer H.C. Sorby described chondrules as “droplets of fiery rain”. In our model of chondrule formation, this description is apt. We have posited that chondrules are the fallout from the collisional disruption of an asteroid.

In a hypervelocity collision, a fraction of the mass of the impactor and target, initially solid, is heated to vaporization. The hot, over-pressured vapor expands, aerodynamically entraining and conductively heating particle debris of various sizes. We have detailed how the vapor cloud evolves

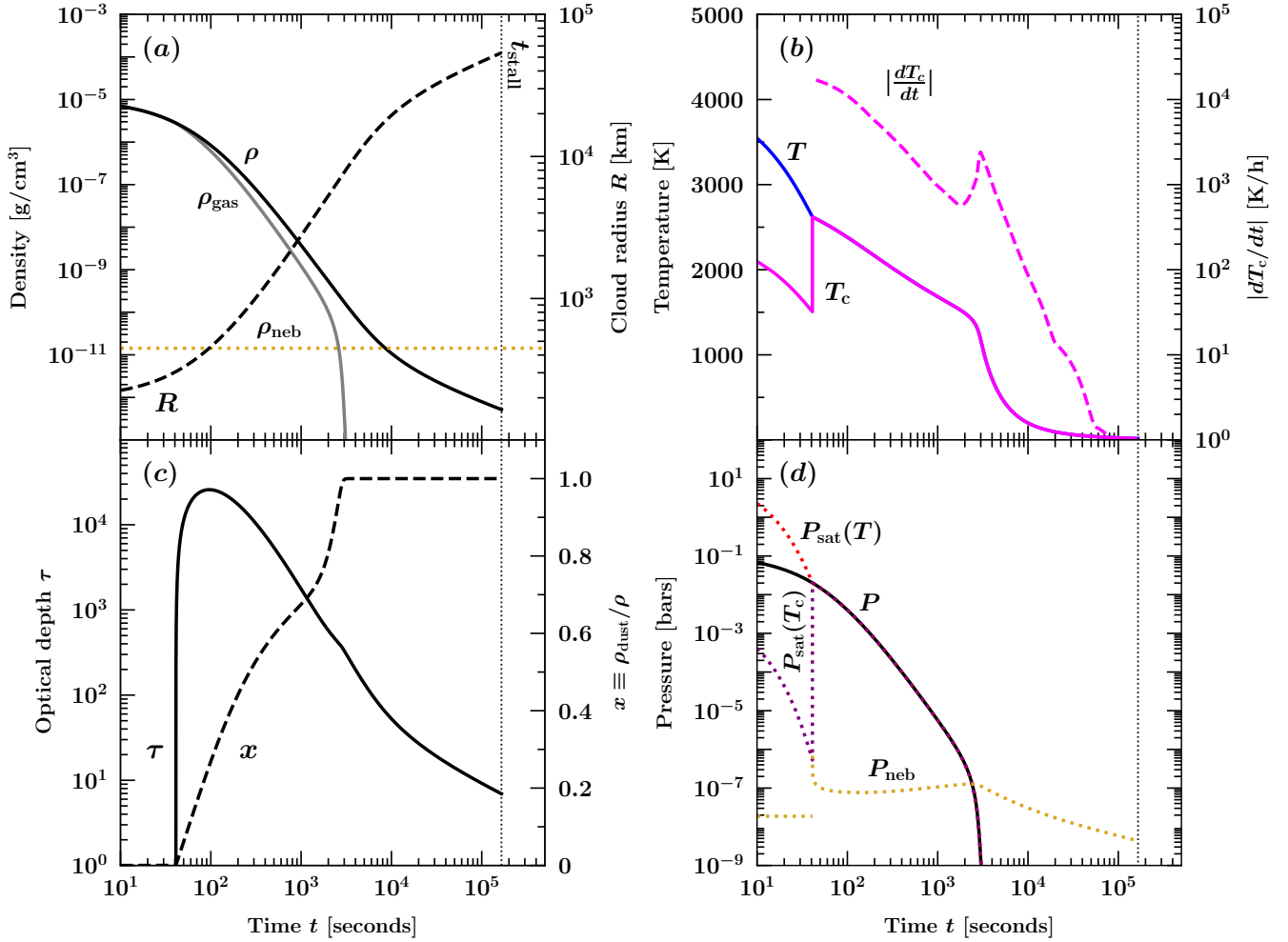


Figure 8. Same as Fig. 1, but for a vapor cloud created at $a = 15$ au in a nebula of density $\rho_{\text{neb}} = 1.4 \times 10^{-11}$ g/cm³, conditions intended to model those of the proto-Kuiper belt where comet Wild-2 may have formed. The change in scenery does not much affect the thermal evolution of either the silicate cloud or the chondrule at temperatures $T \gtrsim 500$ K and times $t \lesssim 5 \times 10^3$ s. The main difference in cloud evolution between asteroid belt and Kuiper belt distances is at late times. Because the nebular pressure P_{neb} is about 2 orders of magnitude lower at 15 au than at 3 au, the cloud takes longer to stall; nebular backfilling begins a factor of ~ 20 later, at $t_{\text{stall}} \sim 10^5$ seconds.

and interacts with the surrounding solar nebula. The evolutionary stages of the cloud include, in chronological and overlapping order: (1) its initial free expansion and adiabatic cooling, (2) its condensation into dust grains whose latent heat slows the cloud’s cooling at first, and whose emitted radiation later hastens it, (3) the cloud’s deceleration due to nebular gas loading, and (4) its eventual collapse and mixing with the nebula, which backfills the near pressure-less cavity left by condensation. Against the evolving backdrop of the vapor cloud we have shown that entrained particles experience heating and cooling episodes consistent with those inferred for chondrules: heating to the point of melting (but not vaporizing) for a period of order 10^2 s; super-liquidus cooling at rates of 3000 K/hr or more; and sub-liquidus cooling at rates of 3000 K/hr to 5 K/hr.

The fact that chondrules fill so much of the volume of some meteorites (Weisberg et al. 2006, their table 1) argues that whatever process heated them went hand-in-hand with whatever process agglomerated them. In our model, heat-

ing and agglomeration—really, re-agglomeration—occur in direct succession in the aftermath of a single collision. Heating and most of the subsequent cooling take place during the above mentioned phases (1)–(3), and re-agglomeration occurs during phase (4). Re-agglomeration starts when nebular gas backfills the cloud cavity and sweeps in particles below a certain size; it completes when particles above a certain size settle gravitationally at drag-limited velocities onto the disrupted planetesimal remains. Particles that are too large fail to be turned around by nebular gas; particles that are too small settle too slowly and do not land before being torn away by solar tides. Those particles that are successfully re-collected have a narrow range of sizes, on the order of a millimeter for nebular densities comparable to that of the minimum-mass solar nebula at the location of the main asteroid belt. At the lower nebular densities thought to prevail in the proto-Kuiper belt, fallback particles are smaller, on the order of $10 \mu\text{m}$.

Raining down chondrules onto the surfaces of their re-

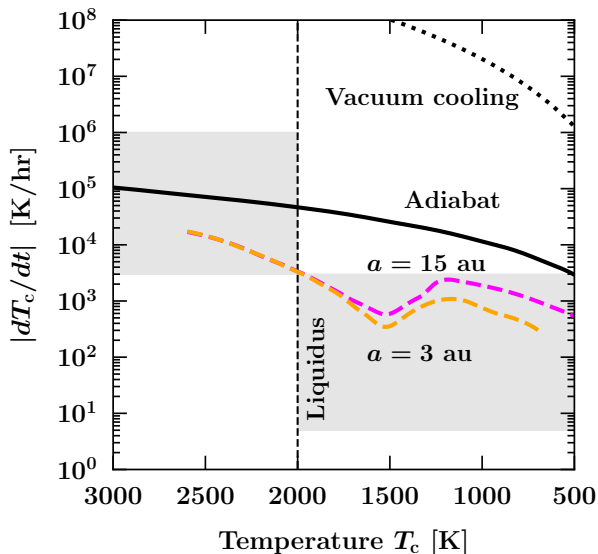


Figure 9. Comparison of chondrule cooling rates at 3 au in the asteroid belt (as in Fig. 2) and at 15 au in the proto-Kuiper belt. Collisional vapor clouds have thermal histories that are practically independent of heliocentric distance and can thus explain the presence of chondrule-like particles discovered by *Stardust*. Cooling is somewhat faster at 15 au than at 3 au because at larger distances the cloud is less impeded by a less dense nebula, and therefore expands faster.

constituted parents manifestly produces the chondritic outer layers of asteroids (Weiss & Elkins-Tanton 2013; see also Asphang et al. 2011 for an early qualitative version of “layering”). Repeated collisions could explain the multiple heating events experienced by an order-unity fraction of chondrules, as evidenced by their having relict grains (melt-grown phenocrysts) from prior heating episodes, and/or igneous rims (e.g. Nagahara 1981; Jones 2012). Chondritic matrix could be the micron-sized dust which condenses from the vapor cloud, situated close enough to the parent body to re-agglomerate before shearing away.

Melting and vaporizing chondritic-composition solids (we used BSE, bulk silicate earth) practically automatically produces the high oxygen fugacities implicated by asteroidal chondrules and chondrule-like particles in comets. For example, given that oxygen makes up 1/10 of BSE vapor by number (Fegley & Schaefer 2012, their fig. 4), we find that oxygen partial pressures (a.k.a. f_{O_2}) for our fiducial vapor cloud in the proto-Kuiper belt are slightly above the iron-wüstite buffer, in agreement with experimentally measured oxygen fugacities for Wild-2 cometary chondrules (Gainsforth et al. 2015). Other fugacity values could be produced by varying the impactor compositions; in most cases they should hew closely to oxygen fugacities found in type I or type II (FeO-poor or rich) chondrules.

In the context of our simple, zero-dimensional model, the total mass M_{cloud} in the vapor cloud must be $\gtrsim 10^{17}$ g to keep chondrule sub-liquidus cooling rates sufficiently low. At the same time, initial vapor densities ρ_0 must be $\lesssim 10^{-3}$ g/cm³ to avoid overly heating chondrules and vaporizing them. These two constraints imply that the initial radius R_0 of the cloud must be $\gtrsim 30$ km. In our model R_0 scales in proportion to the radius of the underlying planetesimal,

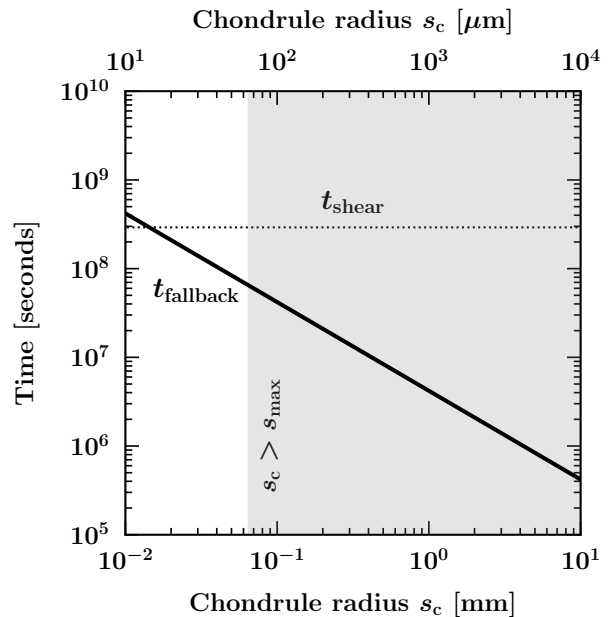


Figure 10. Same as Fig. 3, but for a collision in the proto-Kuiper belt at 15 au. We predict that KBOs contain smaller chondrules than main belt asteroids at 3 au do. The maximum size of retained particles is lower because nebular gas at larger heliocentric distances is less dense and therefore less effective at stopping particle ejecta from being lost to space. The minimum particle size also decreases because tidal forces are weaker at 15 au (t_{shear} is longer by a factor of 30 compared to 3 au), affording smaller particles more time to sediment onto the parent body. Note that the curves plotted here should not be taken too literally as they are sensitive to uncertain order-unity factors (see the end of section 3.2); in particular, t_{fallback} could be lowered by an order of magnitude or more if we consider particles settling from a distance of r_{init} less than our fiducial value of $R_{\text{stall}}/3$.

imal, $R_0 = 2R_{\text{pl}}$; thus we conclude that chondrule formation requires collisions between asteroids $\gtrsim 15$ km in size, with \gtrsim a few hundred km sizes favored to achieve cooling rates $\gtrsim 10^2$ K/hr. By this reasoning, comet Wild-2, which is only 5 km wide, is unlikely to have undergone itself the collision that produced the micro-chondrules it contains. That collision probably occurred for a larger body, which later collided again and fragmented to produce Wild-2. This origin story fits with the idea that short-period comets are collisional fragments (e.g. Farinella & Davis 1996).

It might be objected that planetesimals having sizes $\gtrsim \mathcal{O}(100)$ km would have chemically differentiated from the trapped radiogenic heat from ^{26}Al , in violation of the observation that chondrules are composed of undifferentiated (near-solar composition) material. But as Weiss & Elkins-Tanton (2013) have argued, the outermost portions of even large planetesimals can remain undifferentiated because of surface cooling. Our model requires that collisions thermally re-process more of this outer material into chondrules than the core material; this seems easy enough to satisfy.

At face value, the above parameters imply a vapor-to-planetesimal mass fraction of $f_{\text{vap}} = M_{\text{cloud}}/(4\pi\rho_{\text{solid}}R_{\text{pl}}^3/3) = 7\rho_0/\rho_{\text{solid}} \lesssim 0.2\%$, for a bulk solid density $\rho_{\text{solid}} = 3$ g/cm³. This constraint on f_{vap} is uncertain, however, as it is sensitive to order-unity constants that we have only guessed at.

For example, we could have set the underlying planetesimal radius to $R_{\text{pl}} = R_0/5$, in which case our upper limit on f_{vap} would increase by more than an order of magnitude to $\sim 3\%$ (and to offset the effect of such a choice on the minimum fallback particle size s_{min} and keep its value at 0.2 mm, we would simultaneously reduce $r_{\text{init}}/R_{\text{stall}}$ — the radius from which chondrules start settling after nebular backfilling, scaled to the cavity radius — to 1/8 from our nominal 1/3). Regardless, if we rely solely on the vapor to melt initially solid chondrule precursors (as we have done throughout this paper), then f_{vap} is essentially the maximum efficiency with which a collision converts solid material into chondrules, since the finite heat capacity of the vapor dictates that we cannot melt much more mass in precursors than there is mass in vapor. Efficiencies on the order of a percent are comparable to those reported for melt production by impact jetting, at collision velocities of ~ 3 km/s (Johnson et al. 2015; Wakita et al. 2017).

We worry that efficiencies $f_{\text{vap}} \lesssim 1\%$ may be too small to reprocess enough of the mass of the asteroid belt into chondrules. Repeated collisions might be a way to thicken the depth of the fallout layer. Greater efficiencies of melt production may be achieved through higher impact velocity collisions (Davies et al. 2020). More ab initio simulations of vaporizing collisions, like that by Stewart et al. (2019b), are needed to determine the relative fractions of solid, melt, and vapor initially created by impacts. It seems worthwhile to re-visit the case where initial melt-to-vapor fractions are large (cf. Dullemond et al. 2014, 2016) and incorporate some of our ideas about dust condensation, nebular backfilling, and re-agglomeration. One can also explore the evolution of lower mass, lower temperature, and faster cooling clouds to see if they might generate the equilibrated aggregates (and perhaps also GEMS, glass with embedded metals and sulfides) present in comets (Bradley 1994; Messenger et al. 2013).

Also requiring development are the “big-picture” dynamical histories of the asteroid and proto-Kuiper belts, i.e., how their size and velocity distributions evolve. Our finding that colliding planetesimals need to have sizes $R_{\text{pl}} \gtrsim 15$ km to produce chondrule-like thermal histories, with 100 km or larger sized bodies preferred, aligns with the fact that most of the mass in various minor body reservoirs throughout the Solar System is concentrated at the ~ 100 -km size range (e.g. Morbidelli et al. 2009; Sheppard & Trujillo 2010; Klahr & Schreiber 2020). The super-km/s impact velocities required to produce melt and vapor must arise from gravitational interactions with still larger bodies, e.g. scatterings off lunar-sized embryos populating the primordial asteroid belt (e.g. Wetherill 1992; Petit et al. 2001; O’Brien et al. 2007) or proto-giant planets in the outer solar system (e.g. Tsiganis et al. 2005; Gomes et al. 2005; Carter & Stewart 2020). Note that the scattering (a.k.a. viscously stirring) bodies must have formed with practically the full complement of solar nebular gas still present.

Pending the resolution of these larger issues, we venture to make some predictions that may be testable:

(i) There should be correlations between chondrule ages, maximum sizes, and sub-liquidus cooling rates. Older chondrules (as determined by radiometric dating) were created when the solar nebula was presumably denser and better

able to drag larger particle debris back onto their collisionally disrupted parents (equation 15) — older chondrules should therefore have larger maximum sizes. And insofar as planetesimals were “born big” and became smaller in a collisional cascade (Morbidelli et al. 2009; Klahr & Schreiber 2020), older chondrules should have cooled more slowly, as they were produced in collisions between larger bodies with more massive vapor clouds.

(ii) Asteroidal chondrules and chondrule-like particles in comets should exhibit evidence for slower rates of cooling above a certain temperature, and faster rates below it, following the change in cloud cooling rate before and after the onset of radiative losses. Using Fig. 8b as an example, we see that $T_{\text{rad}} \sim 1400$ K marks the transition to faster radiation-dominated cooling. Phases such as olivine, pyroxene, and spinel that form above T_{rad} would show a relatively narrow range of equilibration temperatures near T_{rad} , because they would be closer to equilibrium when the temperature plummets. Phases such as feldspar and sulfide that form at temperatures below T_{rad} would show poorer equilibrium. By contrast, in a scenario with a constant cooling rate, we would expect a wider spacing between equilibration temperatures as phases freeze out sequentially. Our multi-stage cooling model could explain the results of Gainsforth et al. (2015), who studied one of the chondrule-like particles recovered by *Stardust* (“Iris”) and found that olivine and spinel showed homogenous compositions equilibrated at ~ 1300 K, while feldspar showed a range of compositions consistent with formation from 1300 K down to 1000 K, as well as the presence of glass.

We have made the case that thermally processed solids in asteroids and comets record the early and violent collisional history of the Solar System, including the velocities and sizes of impacting bodies, and how much nebular gas was present. While this information does not directly inform how planetesimals formed, it does constrain formation: according to our calculations, ~ 100 -km sized bodies must have formed and been gravitationally stirred by still larger bodies before the ambient gas density fell much below minimum-mass solar nebular values.

How CAIs (calcium-aluminum-rich inclusions) fit into this framework remains an outstanding question. Compared to chondrules, the igneous CAIs in CV chondrites (1) are older by up to ~ 5 Myr (e.g. Krot et al. 2005; Kita et al. 2005), (2) have larger maximum sizes up to centimeters, and (3) have overlapping cooling rates that skew toward lower values, of order 0.5–50 K/hr (Stolper & Paque 1986; Beckett et al. 2006; see also Connolly Jr. & Jones 2016 for a broader discussion). Encouragingly, these properties match the age-size-cooling trends we articulated above for chondrules. In this picture, large first-generation asteroids would have collided first to create the igneous CAIs, and their smaller collisional progeny would themselves have collided to form the faster cooling chondrules. Like chondrules, CAIs experienced multiple heating events (Connolly & Burnett 1999; Hsu et al. 2000; Kita et al. 2012) that might be explained by multiple collisions. Composition is a problem; how planetesimal collisions would produce fallout with the more refractory compositions of CAIs is unclear. Another problem lies in the detection, modulo significant uncertainty, of excess ^7Li in a CAI from the Efremovka meteorite (Mishra & Marhas 2019;

see also [McKeegan et al. 2000](#), [Chaussidon et al. 2006](#), and [Leya 2011](#)). Lithium-7 is the decay product of ^7Be , whose half-life is just 53 days. The presence of such a short-lived radionuclide at the time of CAI formation would appear to require spallation of CAIs or their precursors by energetic particles emitted by the young Sun. The nucleosynthetic reactions are thought to occur well inside the location of the present-day asteroid belt, perhaps even inside 0.1 AU, depending on the (largely unknown) fluences of protosolar flares (e.g. [Gounelle et al. 2001](#); [Gounelle et al. 2013](#); [Mishra & Marhas 2019](#); see [Jacquet 2019](#) for the case of ^{10}Be). Staging CAI-forming collisions at smaller heliocentric distances would presumably further increase ambient nebular densities and thereby increase the maximum sizes of CAIs. The challenge would be to explain how CAIs were transported radially outward to the asteroid belt.

ACKNOWLEDGEMENTS

We thank Sarah Stewart for an inspiring talk that motivated this work, and Bill Bottke, Don Brownlee, Linda Elkins-Tanton, Sivan Ginzburg, Philipp Kempf, Tomoki Nakamura, Laura Schaefer, and Ben Weiss for useful and encouraging exchanges. We are also grateful to the many people we talked with over the years about chondrules, including Jay Melosh. This work was supported by NASA grant NNX15AD95G/NEXSS and Berkeley's Esper Larsen, Jr. fund.

DATA AVAILABILITY

No new data were generated or analysed in support of this research.

REFERENCES

- Alexander C. M. O. D., Grossman J. N., Ebel D. S., Ciesla F. J., 2008, *Science*, **320**, 1617
- Armitage P. J., 2011, *ARA&A*, **49**, 195
- Asphaug E., Jutzi M., Movshovitz N., 2011, *Earth and Planetary Science Letters*, **308**, 369
- Beckett J. R., Connolly H. C., Ebel D. S., 2006, Chemical Processes in Igneous Calcium-Aluminum-rich Inclusions: A Mostly CMAS View of Melting and Crystallization. p. 399
- Bradley J. P., 1994, *Geochimica Cosmochimica Acta*, **58**, 2123
- Bridges J. C., Changela H. G., Nayakshin S., Starkey N. A., Franchi I. A., 2012, *Earth and Planetary Science Letters*, **341**, 186
- Brownlee D., 2014, *Annual Review of Earth and Planetary Sciences*, **42**, 179
- Brownlee D. E., Joswiak D. J., Bradley J. P., Matrajt G., Wooden D. H., 2005, in Mackwell S., Stansbery E., eds, 36th Annual Lunar and Planetary Science Conference. Lunar and Planetary Science Conference. p. 2391
- Carter P. J., Stewart S. T., 2020, arXiv e-prints, p. [arXiv:2008.05549](#)
- Chaussidon M., Robert F., McKeegan K. D., 2006, *Geochimica Cosmochimica Acta*, **70**, 224
- Chevalier R. A., Fransson C., 2017, Thermal and Non-thermal Emission from Circumstellar Interaction. p. 875, [doi:10.1007/978-3-319-21846-5_34](#)
- Chiang E., Youdin A. N., 2010, *Annual Review of Earth and Planetary Sciences*, **38**, 493
- Connolly Harold C. J., Burnett D. S., 1999, *Meteoritics and Planetary Science*, **34**, 829
- Connolly Jr. H. C., Jones R. H., 2016, *Journal of Geophysical Research: Planets*, **121**, 1885
- Davies E. J., Carter P. J., Root S., Kraus R. G., Spaulding D. K., Stewart S. T., Jacobsen S. B., 2020, *Journal of Geophysical Research (Planets)*, **125**, e06227
- Dawson R. I., Murray-Clay R., 2012, *ApJ*, **750**, 43
- Desch S. J., Connolly H. C. J., 2002, *Meteoritics and Planetary Science*, **37**, 183
- Dullemond C. P., Stammler S. M., Johansen A., 2014, *ApJ*, **794**, 91
- Dullemond C. P., Harsono D., Stammler S. M., Johansen A., 2016, *ApJ*, **832**, 91
- Ebel D. S., Grossman L., 2000, *Geochimica Cosmochimica Acta*, **64**, 339
- Epstein P. S., 1924, *Phys. Rev.*, **23**, 710
- Farinella P., Davis D. R., 1996, *Science*, **273**, 938
- Fedkin A. V., Grossman L., 2013, *Geochimica Cosmochimica Acta*, **112**, 226
- Fegley Bruce J., Schaefer L., 2012, arXiv e-prints, p. [arXiv:1210.0270](#)
- Fernandez J. A., Ip W. H., 1984, *Icarus*, **58**, 109
- Ford E. B., Chiang E. I., 2007, *ApJ*, **661**, 602
- Friedrich J. M., Weisberg M. K., Ebel D. S., Biltz A. E., Corbett B. M., Iotzov I. V., Khan W. S., Wolman M. D., 2015, *Chemie der Erde / Geochemistry*, **75**, 419
- Gainsforth Z., et al., 2015, *Meteoritics and Planetary Science*, **50**, 976
- Gao P., et al., 2020, *Nature Astronomy*, arXiv 2005.11939
- Gomes R., Levison H. F., Tsiganis K., Morbidelli A., 2005, *Nature*, **435**, 466
- Gounelle M., Shu F. H., Shang H., Glassgold A. E., Rehm K. E., Lee T., 2001, *ApJ*, **548**, 1051
- Gounelle M., Chaussidon M., Rollion-Bard C., 2013, *ApJ*, **763**, L33
- Grossman L., Beckett J. R., Fedkin A. V., Simon S. B., Ciesla F. J., 2008, *Reviews in Mineralogy and Geochemistry*, **68**, 93
- Hasegawa Y., Turner N. J., Masiero J., Wakita S., Matsumoto Y., Oshino S., 2016, *ApJ*, **820**, L12
- Hsu W., Wasserburg G. J., Huss G. R., 2000, *Earth and Planetary Science Letters*, **182**, 15
- Huss G. R., Keil K., Taylor G. J., 1981, *Geochimica Cosmochimica Acta*, **45**, 33
- Jacob D., Stodolna J., Leroux H., Langenhorst F., Houdellier F., 2009, *Meteoritics and Planetary Science*, **44**, 1475
- Jacquet E., 2019, *A&A*, **624**, A131
- Johansen A., Mac Low M.-M., Lacerda P., Bizzarro M., 2015, *Science Advances*, **1**, 1500109
- Johnson B. C., Melosh H. J., 2012, *Icarus*, **217**, 416
- Johnson B. C., Melosh H. J., 2014, *Icarus*, **228**, 347
- Johnson B. C., Minton D. A., Melosh H. J., Zuber M. T., 2015, *Nature*, **517**, 339
- Jones R. H., 2012, *Meteoritics and Planetary Science*, **47**, 1176
- Kita N. T., Huss G. R., Tachibana S., Amelin Y., Nyquist L. E., Hutcheon I. D., 2005, in Krot A. N., Scott E. R. D., Reipurth B., eds, Astronomical Society of the Pacific Conference Series Vol. 341, Chondrites and the Protoplanetary Disk. p. 558
- Kita N. T., Ushikubo T., Knight K. B., Mendybaev R. A., Davis A. M., Richter F. M., Fournelle J. H., 2012, *Geochimica Cosmochimica Acta*, **86**, 37
- Klahr H., Schreiber A., 2020, arXiv e-prints, p. [arXiv:2007.10696](#)
- Krot A. N., Wasson J. T., 1995, *Geochimica Cosmochimica Acta*, **59**, 4951
- Krot A. N., Amelin Y., Cassen P., Meibom A., 2005, *Nature*, **436**, 989

- Levison H. F., Morbidelli A., Tsiganis K., Nesvorný D., Gomes R., 2011, *AJ*, **142**, 152
- Leya I., 2011, *Geochimica Cosmochimica Acta*, **75**, 1507
- Lin J. W., Lee E. J., Chiang E., 2018, *MNRAS*, **480**, 4338
- Lock S. J., Stewart S. T., Carter P. J., Davies E. J., Petaev M. I., Jacobsen S. B., 2019, in Lunar and Planetary Science Conference. Lunar and Planetary Science Conference. p. 1783
- Malhotra R., 1995, *AJ*, **110**, 420
- McKeegan K. D., Chaussidon M., Robert F., 2000, *Science*, **289**, 1334
- Melosh H. J., 1989, Impact cratering : a geologic process
- Messenger S., Keller L. P., Nguyen A. N., 2013, in Proceedings of The Life Cycle of Dust in the Universe: Observations. p. 40
- Mishra R. K., Marhas K. K., 2019, *Nature Astronomy*, **3**, 498
- Morbidelli A., Bottke W. F., Nesvorný D., Levison H. F., 2009, *Icarus*, **204**, 558
- Nagahara H., 1981, *Nature*, **292**, 135
- Nagahara H., Kushiro I., Mysen B. O., 1994, *Geochimica Cosmochimica Acta*, **58**, 1951
- Nakamura T., et al., 2008, *Science*, **321**, 1664
- Nesvorný D., Vokrouhlický D., Dones L., Levison H. F., Kaib N., Morbidelli A., 2017, *ApJ*, **845**, 27
- O'Brien D. P., Morbidelli A., Bottke W. F., 2007, *Icarus*, **191**, 434
- Ormel C. W., 2017, The Emerging Paradigm of Pebble Accretion. p. 197, doi:10.1007/978-3-319-60609-5_7
- Petit J.-M., Morbidelli A., Chambers J., 2001, *Icarus*, **153**, 338
- Russell S., Connolly H., Krot A., 2018, Chondrules: Records of Protoplanetary Disk Processes. Cambridge Planetary Science, Cambridge University Press, doi:10.1017/9781108284073
- Sanders I. S., Scott E. R. D., 2012, *Meteoritics and Planetary Science*, **47**, 2170
- Sheppard S. S., Trujillo C. A., 2010, *ApJ*, **723**, L233
- Shu F. H., 1992, The physics of astrophysics. Volume II: Gas dynamics.
- Stewart S. T., Carter P. J., Davies E. J., Lock S. J., Kraus R. G., Root S., Petaev M. I., Jacobsen S. B., 2019a, in Lunar and Planetary Science Conference. Lunar and Planetary Science Conference. p. 1250
- Stewart S. T., Carter P. J., Davies E. J., Lock S. J., Kraus R. G., Root S., Petaev M. I., Jacobsen S. B., 2019b, in Lunar and Planetary Science Conference. Lunar and Planetary Science Conference. p. 1251
- Stolper E., Paque J. M., 1986, *Geochimica Cosmochimica Acta*, **50**, 1785
- Tsiganis K., Gomes R., Morbidelli A., Levison H. F., 2005, *Nature*, **435**, 459
- Villeneuve J., Libourel G., Soulié C., 2015, *Geochimica Cosmochimica Acta*, **160**, 277
- Wakita S., Matsumoto Y., Oshino S., Hasegawa Y., 2017, *ApJ*, **834**, 125
- Weidenschilling S. J., 1977, *MNRAS*, **180**, 57
- Weisberg M. K., McCoy T. J., Krot A. N., 2006, Systematics and Evaluation of Meteorite Classification. p. 19
- Weiss B. P., Elkins-Tanton L. T., 2013, *Annual Review of Earth and Planetary Sciences*, **41**, 529
- Wetherill G. W., 1992, *Icarus*, **100**, 307
- Williams J. P., Cieza L. A., 2011, *ARA&A*, **49**, 67
- Zel'dovich Y. B., Raizer Y. P., 1967, Physics of shock waves and high-temperature hydrodynamic phenomena

This paper has been typeset from a $\text{\TeX}/\text{\LaTeX}$ file prepared by the author.